Naval Research Laboratory
Washington, DC 20375-5320

NRL/7330/MR—2021/2

Acoustic Doppler Current Profiler Velocity and Relative Backscatter Anomaly Error Analysis and Error Propagation

SABRINA M. PARRA

Applied Physics Laboratory
Johns Hopkins University
Laurel, MD

JEFFREY W. BOOK

Physical Oceanographic Processes Section
Ocean Sciences Division

October 26, 2021

REPORT DOCUMENTATION PAGE

Form Approved
OMB No. 0704-0188

1. REPORT DATE *(DD-MM-YYYY)*	**2. REPORT TYPE**	**3. DATES COVERED** *(From - To)*
26-10-2021	NRL Memorandum Report	08-07-2015 – 09-30-2021

4. TITLE AND SUBTITLE

Acoustic Doppler Current Profiler Velocity and Relative Backscatter Anomaly Error Analysis and Error Propagation

5a. CONTRACT NUMBER

5b. GRANT NUMBER

5c. PROGRAM ELEMENT NUMBER

6. AUTHOR(S)

Sabrina M. Parra* and Jeffrey W. Book

5d. PROJECT NUMBER

5e. TASK NUMBER

5f. WORK UNIT NUMBER
1D90

7. PERFORMING ORGANIZATION NAME(S) AND ADDRESS(ES)

Naval Research Laboratory
Ocean Sciences Division
Stennis Space Center, MS 39529-5004

8. PERFORMING ORGANIZATION REPORT NUMBER

NRL/7330/MR--2021/2

9. SPONSORING / MONITORING AGENCY NAME(S) AND ADDRESS(ES)

The Gulf of Mexico Research Initiative
1141 Bayview Ave.
Biloxi, MS 39530

10. SPONSOR / MONITOR'S ACRONYM(S)

GOMRI

11. SPONSOR / MONITOR'S REPORT NUMBER(S)

12. DISTRIBUTION / AVAILABILITY STATEMENT

DISTRIBUTION STATEMENT A: Approved for public release; distribution is unlimited.

13. SUPPLEMENTARY NOTES

*Formerly American Society for Engineering Education and the University of Southern Mississippi
Applied Physics Laboratory, Johns Hopkins University, 11100 Johns Hopkins Road, Laurel, Maryland 20723-6099

14. ABSTRACT

Five acoustic Doppler current profilers (ADCPs) were moored to the bottom on the northern Gulf of Mexico shelf from early November 2015 through mid-April 2016. The acoustic backscatter and vertical velocity profiles were used to qualitatively estimate zooplankton concentrations and their vertical velocities during diel vertical migrations. Error analysis and error propagation was performed for the vertical velocities and for each term of the backscatter anomaly equation at the five mooring locations. Four of the ADCPs were 300 kHz Teledyne Workhorse Sentinel measuring continuously every 12 seconds. Another was a 600 kHz ADCP measuring hourly bursts of 10 min at 1 Hz. The vertical velocity errors for hourly averages were of the order of the vertical velocity magnitudes and slightly higher at the bursting ADCP location. However, daily and monthly averaging lowered the vertical velocity errors by at least one order of magnitude. The errors associated with the relative backscatter anomalies were broken down by each relevant term of the backscatter equation. As the errors propagated through the equation and the averaging, the error magnitudes were at least one order of magnitude smaller than the relevant variations. Errors at least one order of magnitude smaller than the signals of interest confirm that the observed diel signals were valid.

15. SUBJECT TERMS

16. SECURITY CLASSIFICATION OF:			**17. LIMITATION OF ABSTRACT**	**18. NUMBER OF PAGES**	**19a. NAME OF RESPONSIBLE PERSON**
					Jeffrey W. Book
a. REPORT	**b. ABSTRACT**	**c. THIS PAGE**	U	34	**19b. TELEPHONE NUMBER** *(include area code)*
U	U	U			(228) 688-5251

Standard Form 298 (Rev. 8-98)
Prescribed by ANSI Std. Z39.18

This page intentionally left blank.

CONTENTS

LIST OF FIGURES

LIST OF TABLES

ACOUSTIC DOPPLER CURRENT PROFILER VELOCITY AND RELATIVE BACKSCATTER ANOMALY ERROR ANALYSIS AND ERROR PROPAGATION

1. ABSTRACT

Five acoustic Doppler current profilers (ADCPs) were moored to the bottom on the northern Gulf of Mexico shelf from early November 2015 through mid-April 2016. The acoustic backscatter and vertical velocity profiles were used to qualitatively estimate zooplankton concentrations and their vertical velocities during diel vertical migrations. Error analysis and error propagation was performed for the vertical velocities and for each term of the backscatter anomaly equation at the five mooring locations. Four of the ADCPs were 300 kHz Teledyne Workhorse Sentinel measuring continuously every 12 seconds. Another was a 600 kHz ADCP measuring hourly bursts of 10 min at 1 Hz. The vertical velocity errors for hourly averages were of the order of the vertical velocity magnitudes and slightly higher at the bursting ADCP location. However, daily and monthly averaging lowered the vertical velocity errors by at least one order of magnitude. The errors associated with the relative backscatter anomalies were broken down by each relevant term of the backscatter equation. As the errors propagated through the equation and the averaging, the error magnitudes were at least one order of magnitude smaller than the relevant variations. Errors at least one order of magnitude smaller than the signals of interest confirm that the observed diel signals were valid.

2. INTRODUCTION

The Naval Research Laboratory is part of the CONsortium for Oil Spill Exposure Pathways in COastal River-Dominated Ecosystems (CONCORDE). CONCORDE is a highly interdisciplinary consortium funded by the Gulf of Mexico Research Initiative with the aim to expand the understanding of oil transport pathways and exposure in the complex inner- and mid-shelf regions in the river-dominated northern Gulf of Mexico shelf (Greer et al., 2018). The work included an extended mooring deployment in the northern Gulf of Mexico shelf of five bottom moorings from early November 2015 through mid-April 2016 (Table 1, Figure 1). The bottom moorings consisted of a trawl resistant Barny Sentinel design (Perkins et al., 2000) for protection from the extensive fishing and commercial boating activities in this region. Each mooring was equipped with an upward-looking, Teledyne Workhorse Sentinel acoustic Doppler current profiler (ADCP) and a Seabird 26 or 26+ wave-tide gauge (WTG). The WTG deployed at C1 failed ~3 hours after deployment and is therefore not considered in this report. The daily variations of the backscatter and vertical velocity profiles were used to understand the diel vertical migrations of zooplankton (Parra et al., 2019). Backscatter, estimated from the echo intensity from the ADCPs, can be used to qualitatively estimate concentrations of zooplankton and observe their movements in the water column. The vertical velocities can be representative of the bulk vertical swimming velocities of zooplankton (Heywood, 1996; Jiang et al., 2007; La et al., 2015). This report presents a formal error analysis and investigation into the error propagation to confirm the validity of the vertical velocity and relative backscatter observations.

3. ADCP RANDOM ERRORS

For a ~6 month deployment with single lithium battery packs, 2 GB memory cards, and the scientific objective of measuring ~70 m of the water column at 1 m depth resolution, a 300 kHz Teledyne

Manuscript approved October 1, 2021.

Workhorse Sentinel can store about 300 ensembles per hour and make about 1000 acoustic ping measurements per hour. Therefore, four ADCPs (300 kHz at C1-C3, and C5) were programmed to measure continuous ensembles every 12 seconds (Table 1), maximizing the memory card storage that was available. Each 12 second ensemble consisted of the average of only three pings (one every four seconds) to stay within the available power budget. In order to observe higher frequency variability, one ADCP (600 kHz at C4) was set to hourly bursts of 10 minutes at 2 Hz with 1 Hz ensemble storage (Table 1). The depth resolution for this ADCP was reduced to 1.5 m to preserve power and extend the range of the 600 kHz instrument. The high frequency of measurement at C4 allowed for the observation of wave orbital velocities and the estimation of turbulence. However, the burst measurement scheme that was used at C4 aliases energy at periods between twice the burst repeat period and the burst duration (10 minute < aliased period ≤ 2 hours) into longer periods of the burst sampled time series. The continuous sampling scheme also aliases wave energy at frequencies 0.125 Hz and higher into lower frequencies, but the errors associated with this wave energy aliasing are not considered in this report. The profiles of velocity and echo intensity were high-pass filtered with a cutoff frequency of 2/3 day^{-1} (36 hour period) using a fast Fourier transform filter with Hanning windowing to remove unrelated processes of longer duration than zooplankton daily migrations. The random error for the horizontal and vertical velocity, as well as for the echo intensity profiles can be estimated for all the moorings through different techniques.

3.1 Velocity error profiles

The ADCP velocity data contains inaccuracies attributed to internal and external biasing error, and random error. The random errors associated with the Workhorse Sentinel ADCP measurements can be statistically estimated from the redundancy of a four beam ADCP angled at $\theta = 20°$ from the vertical (Teledyne RDI, 2010, 2011). Each beam measures a radial velocity that when combined with other beam radials can be transformed into horizontal, vertical, and "error" velocity components. The transforms are (Teledyne RDI, 2010, equation 9):

$$V_x = \frac{b_1 - b_2}{2 \sin\theta} \quad (1)$$

$$V_y = \frac{b_4 - b_3}{2 \sin\theta} \quad (2)$$

$$V_z = \frac{b_1 + b_2 + b_3 + b_4}{4 \cos\theta} \quad (3)$$

$$V_e = \frac{b_1 + b_2 - b_3 - b_4}{2\sqrt{2} \sin\theta} \quad (4)$$

where $b_{1\text{-}4}$ are the respective beam radials at a given depth level, V_x and V_y are the horizontal velocity components, V_z is the average of two independent vertical velocity estimates, and V_e is a scaled difference of the two independent vertical velocity estimates(Teledyne RDI, 2010, section 5.3). The scaling is chosen so that the standard deviation of V_e is equal to the expected random error of the horizontal velocity measurements, $\frac{\sigma_b}{\sqrt{p}\sqrt{2}\sin\theta}$. The expected random error of the vertical velocity measurement is $\frac{\sigma_b}{\sqrt{p}\,2\cos\theta}$. The p term accounts for the averaging of multiple pings per stored ensemble.

Therefore, the error velocity, V_e, can be used to calculate the expected random errors for horizontal, σ_{horz}, and vertical, σ_{vert}, velocity ensemble averages with the following equations:

$$\sigma_{horz} = \frac{std(V_e)}{\sqrt{s}} \quad (5)$$

$$\sigma_{vert} = \frac{tan\,\theta}{\sqrt{2}}\sigma_{horz} \quad (6)$$

where *s* is the number of averaged ensembles. The time series were averaged every 10 minutes for the continuous ADCPs and hourly for the burst measurements at C4. This resulted in averaged ensembles of 50 and 600, respectively. The resulting profiles of σ_{horz} are plotted in Figure 2. This represents the error profiles for the horizontal velocities. Equation (6) was used to convert these to vertical velocity error profiles (not shown) which reduces their magnitudes by a factor of 0.26 compared to the horizontal velocity errors. Before calculating the standard deviation of V_e, the upper-most bins for these upward looking ADCPs were truncated because they are contaminated by side-lobe reflections from the sea-surface. Side-lobe contamination for a non-tilted ADCP should be the range of the ADCP to the sea surface multiplied by $(1 - \cos\theta)$, which for these depths is 3-4 m below the sea surface. Based on quality control variables measured by the ADCPs, additional depth truncation was performed to conservatively remove any possible contamination from the side lobes near the surface. Additional quality control checks were done to exclude potential bad ensembles from these calculations. For all stations except C4, ensembles were accepted if 2 out of 3 pings were marked good by internal checks for all 4 beams, with the exception of the uppermost usable bin near the surface where all 3 pings for all 4 beams had to be marked good to accept the ensemble. For station C4, both pings for all 4 beams had to be marked good for the ensemble to be accepted, regardless of the depth bin level. Velocity errors were significantly higher near the surface, caused by a combination of side lobe interference, surface waves, and surface wave generated bubbles, to name a few (Teledyne RDI, 2011). The velocity errors at C4 were considerably lower than at the other locations because the averaging included many more ensembles (one order of magnitude more) when compared to the continuous time series at the other sites (Table 1). However, the error in Figure 2 for C4 does not account for burst sampling error, which will be analyzed in Section 3.3.

3.2 Echo intensity error profiles

Similar error profiles were calculated for the echo intensity of the ADCPs, however, through a different method. The error of the echo intensity was obtained from the spectral white noise floor. At high frequencies, the spectrum becomes saturated by noise and converges to the white noise level (flattening toward high frequencies) (Durgesh et al., 2014; Richard et al., 2013),

$$\sigma_{echo} = \frac{std(EI_{hi})\sqrt{\frac{N_q}{N_q - f_c}}}{\sqrt{s}} \quad (7)$$

where N_q is the Nyquist frequency equal to half the sampling frequency. For the 300 and 600 kHz ADCPs, a cutoff frequency, f_c, of 0.03 and 0.3 Hz, respectively, was used to represent the noise floor (Figure 3). The echo intensity time series were high-pass filtered (EI_{hi}) at the respective cutoff frequency. The variance of the measured signal, in this case the echo intensity, is the integral of the noise level over the spectral bandwidth. This methodology depends on the assumption that the inverse of the signal to noise ratio is normally distributed about a mean signal to noise ratio. Echo errors were highest near the bottom, bottoming out toward the surface before increasing nearest the surface (Figure 4). The echo errors

were much lower at C4 because of the same reason as for the velocity errors in the previous section. However, the error at C4 does not account for errors associated with burst sampling.

3.3 Burst sampling error

In addition to the error attributed to measurement and instrument inaccuracies, error is also introduced through a burst sampling scheme. Burst sampling introduces error in the estimation of hourly mean values for C4. The error originates from the aliasing of energy between the burst duration and the period between bursts. In our case, the mooring at C4 performed hourly bursts of 10 minutes at 1 Hz. The other moorings measured continuously every 12 seconds. Here we used the continuous time series to estimate the aliasing of the burst sampling, and understand the differences between the two sampling schemes.

The time series at C5 illustrate the difference between the two sampling schemes in Figure 5. Two versions of time series were compared: (a) hourly means of the 12 second interval data (blue line in Figure 5), and (b) averaging the first 10 minutes of each hour as a representation of the hourly bursts at C4 (orange line in Figure 5). The difference between these two types of hourly sampling schemes (black line in Figure 5) represent the error associated with burst sampling. The burst sampling error, σ_{burst}, was quantified with the following (Book et al., 2007):

$$\sigma_{\text{burst}} = \sqrt{\sigma_{diff}^2 - \frac{N-1}{N}\sigma_{error}^2} \tag{8}$$

$$\sigma_{\text{diff}} = std(burst - hourly) \tag{9}$$

where *burst* represents the hourly burst time series, *hourly* represents the hourly continuous time series, N is the number of values averaged over 10 minute from the continuous hourly averaging (in this case 6, i.e., a value every 10 minutes). I.e., the variance of the difference between the time series, σ_{diff}^2, is a sum of the variance associated with burst sampling, σ_{burst}^2, and the measurement error variance associated with the hourly averages of the continuous time series. The largest burst associated errors appear to be found for the vertical velocities, where the range of variability was similar between the vertical velocities and its error. Echo intensity error was relatively small, except during periods of sharp changes (see the sharp drop in the middle of the day on February 3 in Figure 5). The horizontal velocity burst errors were at least one order of magnitude smaller than the horizontal current variations, while for vertical velocities they were on the same range (Figure 6). For the echo, the burst error magnitudes were one order of magnitude smaller than the variations. Burst sampling error estimates were very consistent for all variables independent of which mooring was used to make the estimate.

The burst sampling error was included into the total error at C4 with (Harris, 2010, pg. 56):

$$\sigma_{\text{C4}} = \sqrt{\sigma_{burst}^2 + \sigma_{inst}^2} \tag{10}$$

where σ_{inst} represents the previously computed errors from equations (5,6,7) for their respective variable. Taking this burst error into account for C4 data, the updated error profiles at C4 in addition to the other moorings are shown in Figure 7. The error at C4 for the horizontal velocities became almost three times larger than the C4 error excluding burst sampling error. When including the burst sampling error, the horizontal velocity error at C4 was around 1.5 times as large as the other moorings. For vertical velocities,

the error at C4 falls within the range of the other moorings. In the case of the echo intensity, the error at C4 became one order of magnitude larger than the rest.

3.4 Monthly and overall daily vertical velocity error propagation

Vertical velocity profiles were reorganized as a function of hour of the day (using a constant time base of UTC–6 to avoid issues with Daylight Savings Time) and depth, with a window for each day. These daily vertical velocity windows were averaged for each month producing monthly averages of the daily depth variations (Figure 8). These were also averaged over the deployment period (Figure 9). This additional averaging further reduced the vertical velocity errors to 0.05 to 0.1 cm/s for the monthly maps and 0.02 to 0.04 cm/s for the overall average maps.

4. RELATIVE BACKSCATTER ERROR

The echo intensity obtained from the ADCP represents the scattering intensity of suspended particles (sediment, biota, bubbles) in the water (Teledyne RDI, 2011). It can be used as a proxy for scatterer (i.e. zooplankton) concentrations in the water. Translating echo intensity into relative backscatter requires knowledge of several variables that may affect the signal intensity: power transmitted to the water, acoustic characteristics of the transducer and acoustic beam, power attenuation resulting from beam spreading and absorption, and properties of the receiver (Deines, 1999). The relative volume backscattering strength, S_v, equation is as follows (Gostiaux & van Haren, 2010, equation 8):

$$S_v = A + 10\,log_{10}\left(\frac{R^2}{r_o^2}\right) + 2\alpha R + 10\,log_{10}\left(10\frac{K_c E_M}{10} + 10\frac{K_c E_N}{10}\right) \tag{11}$$

where A is an unknown constant for a given ADCP, R represents the slant-range distance to the sample bin (m), r_o is the reference distance of 1 m from the transducer, α is the absorption coefficient of seawater (dB/m), K_c is the sensitivity coefficient of the ADCP (0.45 dB/count), E_M is the measured echo intensity by the ADCP (counts), and E_N is the intensity of the ambient noise (counts).

In this equation, S_v is not linearly associated with the measured echo intensity, E_M, however, by performing a Taylor series expansion on each of the two terms in the parenthesis and ignoring all terms of second order and higher results in (for detailed calculations see Web Appendix in Parra et al., 2019):

$$S_v = A + 10\,log_{10}\left(\frac{R^2}{r_o^2}\right) + 2\alpha R + K_c E_M - \frac{10}{\ln(10)}\frac{N}{S} \tag{12}$$

where N is the ambient noise and S is the volume backscattering signal, both recorded by the ADCP (Gostiaux & van Haren, 2010).

4.1 First term: $\mathbf{10\,log_{10}\left(\frac{R^2}{r_o^2}\right)}$

The first term on the right hand side of equation (12) contains the variable R, which represents the slant-range distance of the bins to the profiler. It is calculated using the following formula (Deines, 1999; Lorke et al., 2004):

$$\mathrm{R} = \frac{1}{cos\theta}\left(B + \left(\frac{L - dz}{2}\right) + Ndz + \frac{dz}{4}\right) \tag{13}$$

where B is the blanking distance (m), L is the sum of the transmit pulse length and lag distance (m), dz is

the bin size (m), and *N* is the number of the bin (increasing away from the ADCP). The profiles of *R* linearly increase toward the surface at each mooring (Figure 10).

The error associated with *R* is with respect to the speed of sound of seawater. The ADCP calculates the speed of sound based on the temperature at the transducer head and an estimated constant salinity that is provided at the time the ADCP is programmed for deployment (Teledyne RDI, 2011). Both speed of sound terms were calculated as follows:

$$\mathrm{SoS} = 1449.2 + 4.6T - 0.055T^2 + 0.00029T^3 + (1.34 - 0.01T)(S - 35) + 0.016D \quad (14)$$

where *T* is the temperature (degrees Celsius), *S* is the salinity (psu), and *D* is the depth of the ADCP (m) (Teledyne RDI, 2011). Uncertainty is created by the difference in the speed of sound between the one recorded by the ADCP with constant salinity and the true speed of sound (in this case measured by the wave-tide gauge, Figure 11). This error is quantified as (Harris, 2010, pg. 56):

$$\sigma_R = \frac{R\sigma_{SoS}}{\overline{SoS_{ADCP}}} \quad (15)$$

$$\sigma_{\mathrm{SoS}} = std(SoS_{ADCP} - SoS_{WTG}) \quad (16)$$

where σ_{SoS} is the error associated with the speed of sound, SoS_{WTG} is the speed of sound at the WTG, and SoS_{ADCP} is the speed of sound at the ADCP assuming constant salinity of 35 psu (Figure 10). The WTG at C1 failed so the salinity time series from the WTG at C2 was also used for C1. The error of *R* propagates into the logarithmic term, which is quantified with the following (Harris, 2010, pg. 56):

$$\sigma_{10\log_{10}\left(\frac{\mathrm{R}^2}{r_o^2}\right)} = 10\sigma_{\log_{10}\left(\frac{\mathrm{R}^2}{r_o^2}\right)} = 10\frac{2\sigma_R}{Rln10} = \frac{20\sigma_{SoS}}{\overline{SoS_{ADCP}}ln10} \quad (17)$$

which yields a scalar uncertainty value valid for all bin ranges (orange line in Figure 12) as all error dependence on *R* cancels out. This error term is relatively insignificant compared to error contributions from other terms in Equation 12.

4.2 Second term: $2\alpha R$

The second term on the right hand side of the relative backscatter equation (12) is the product of the sound absorption of seawater, α, and the vertical distance of the bins, *R*. The sound absorption of seawater was calculated following the equations in Francois and Garrison (1982) in Figure 7 with bottom temperature and salinity from the WTG. The values of sound absorption change based on temperature and salinity, therefore, the presence of a freshwater plume at the surface would change the sound absorption profile, and was a source of error. To estimate the error in the sound absorption, simulated temperature and salinity profiles from a numerical model of this region were used (for a description of the Navy Coastal Ocean Model that was used see Greer et al., 2018). The bottom sound absorption of sea water compared relatively well between the WTG and the model estimates (Figure 13), therefore the numerical model results for the region are an acceptable representation of the water properties during the deployment.

The error associated with the vertical profile of the sound absorption of seawater is quantified with:

$$\sigma_\alpha = std\left(\frac{\int_b^{z_o} \alpha dz}{z_o - b} - \alpha(t,b)\right) \quad (18)$$

where z_o represents the depth at each bin, and b represents the depth at the bottom. This equation was applied using the numerical model estimates for each mooring location (Figure 14). The errors were similar between the sites, ranging between 0 dB/m at the bottom to nearly 0.4 dB/m at the surface.

Using the error of α, the error of the second term becomes (Harris, 2010, pg. 56):

$$\sigma_{2\alpha R} = 2\sigma_{\alpha R} = 2\sqrt{(\sigma_\alpha R)^2 + (\sigma_R \alpha)^2} \quad (19)$$

Individual terms for this equation are plotted in Figure 15 and the total error from Equation 19 is plotted as blue lines in Figure 12. The error associated with the $\sigma_R \alpha$ term is removed when the high-pass filter is applied (see Section 3) because the correlation time scale of α for this region was 17.5 days.

4.3 Third term: $K_c E_M$

The error associated with the third term on the right hand side of equation (12) is equivalent to that observed in the bottom row of Figure 7 multiplied by $K_c = 0.45$. See the profiles of the third term plotted as yellow in Figure 12.

4.4 Fourth term: $\frac{10}{\ln(10)}\frac{N}{S}$

The error associated with the fourth and last term on the right hand side of equation (12) is removed by the high-pass filter (see Section 3), and, therefore, it is not included in our calculations.

4.5 Total error of the relative backscatter

The total relative backscatter error for each of the three terms on the right hand side of equation (12) were compiled together as:

$$\sigma_{S_v} = \sqrt{\sigma^2_{10\log_{10}\left(\frac{R^2}{r_o^2}\right)} + \sigma^2_{2\alpha R} + \sigma^2_{K_c E_M}} \quad (20)$$

and represented in Figure 12 in purple. The relative backscatter error is dominated by the second (third) term in the shallower (deeper) half of the water column, except at C4 where the third term always dominates.

4.6 Monthly and overall daily relative backscatter error propagation

Similar to the vertical velocity profiles mentioned in Section 3.4, relative backscatter anomaly profiles were reorganized as a function of hour of the day (using a constant time base of UTC–6 to avoid issues with Daylight Savings Time) and depth, with a window for each day. These daily relative backscatter anomaly windows were averaged for each month producing monthly averages of the daily variations with depth (Figure 8). These were also averaged over the deployment period (Figure 9). This additional averaging further reduced the relative backscatter errors to 0.01 to 0.03 dB (0.16 to 0.23 dB for C4) for the monthly maps, and 0.004 to 0.015 dB (0.07 to 0.1 dB for C4) for the overall average maps.

5. TIME AUGMENTED EOF ERROR PROPAGATION

The errors associated with the high-pass filtered vertical velocity and relative backscatter anomaly also propagated into the empirical orthogonal function (EOF) analysis. Daily windows of high-pass filtered relative backscatter and vertical velocity time series were analyzed with an extended, time-augmented EOF method. Typical EOF analysis (Emery & Thomson, 2001) identifies orthogonal combinations (or modes) of time-varying variables that define new base functions (the modes). The first mode describes the maximum possible variance of the total variable set that can be described by a single linear combination of the variables. The second mode, when combined with the first mode, describes the maximum variance that can be described by the sum of only two orthogonal combinations of variables, and so on. This analysis can identify particular combinations of variables (spatial pattern modes) that co-vary and explain large percentages of the total temporal variability. An extended EOF analysis adds a number of time-lagged and/or time-advanced versions of the variables into the analysis and thus allows the method to describe spatial patterns with set patterns of time evolution. This version of an EOF analysis can be very helpful in finding patterns in variables with known fixed frequencies of variation like the 24-hour patterns of diel vertical migrations.

In this paper, we follow the extended time-augmented EOF analysis method of Book et al. (2016), which is a modification of the extended EOF method presented by Fraedrich et al. (1993). The high-pass filtered relative backscatter anomaly and vertical velocity data were reorganized into daily windows (161 in total), producing windows of hour of the day (UTC-6) and depth for each particular day for each variable. Before calculating the time-augmented EOFs, the mean of the 161 daily windows was calculated and subtracted from each daily window of relative backscatter and vertical velocity. Then, an extended time-augmented EOF analysis was used to find set patterns of how these daily windows varied over the longer time-periods of the mooring deployment. For example, instead of needing 161 (number of complete deployment days) of these windows per mooring to describe the daily variation of relative backscatter anomaly patterns, only three windows (i.e., modes) per mooring can be used to describe the main variance of the daily backscatter patterns. The daily windowed relative backscatter anomaly and vertical velocity profiles from all five moorings were concatenated into one inclusive matrix for the EOF analysis. The results show the covarying dominant modes of variability observed in the relative backscatter anomaly and vertical velocity profiles at all the moorings.

The EOF results also include the error, as it propagated through the calculations. The EOF error was estimated by applying a bootstrap method using 100 EOF ensemble runs. The data used in the 100 ensemble runs included random errors normalized to the error profiles of relative backscatter anomaly (Figure 12) and vertical velocity (Figure 7). The EOF error was calculated relative to the original EOF (EOF_0, without the additional random normalized error) as follows:

$$\sigma_{EOF} = \sqrt{\overline{\left(EOF_0 - EOF_{err,i}\right)^2}} \tag{21}$$

where *i* denotes the ensemble run, and the overbar represents averaging of the 100 ensembles. The results were separated by mooring and mode. For the 300 kHz ADCPs, modes 1 through 3 had backscatter errors less than 0.06, 0.09, and 0.12 dB, respectively (Figure 16). For the 600 kHz ADCP at C4 measuring in hourly bursts, modes 1 through 3 had relative backscatter anomaly errors approximately six times larger than the 300 kHz ADCPs, which measured continuously. At all the ADCPs, modes 1 through 3 had vertical velocity errors less than 0.03, 0.04, and 0.05 cm/s, respectively (Figure 17). The estimated errors in the temporal amplitudes of the three EOF modes were all below 0.001 (Figure 18).

6. CONCLUSIONS

The error analysis and error propagation of the vertical velocity and relative backscatter anomaly profiles confirmed that the observed signals were valid, relative to the errors associated with the measurements. The zooplankton diel vertical migration analysis in Parra et al. (2019) was based on monthly and time-series wide averages as well as EOF analysis. The error associated with these methods were at least one order of magnitude smaller than the signals of interest.

7. ACKNOWLEDGEMENTS

Thanks to everyone involved in CONCORDE, and the crews of the research vessels Point Sur and Pelican. This research was made possible by a grant from The Gulf of Mexico Research Initiative. Data are publicly available through the Gulf of Mexico Research Initiative Information & Data Cooperative at https://data.gulfresearchinitiative.org, doi: 10.7266/N79C6VGW (ADCPs) and 10.7266/N77D2SRV (wave-tide gauges). S.M. Parra is grateful for funding provided from the U.S. Naval Research Laboratory through an American Society for Engineering Education postdoctoral fellowship.

8. REFERENCES

Book, J. W., Jones, N. L., Lowe, R. J., Ivey, G. N., Steinberg, C. R., Brinkman, R. M., Rice, A.E., Bluteau, C.E., Smith, S.R., Smith, T.A., & Matt, S. (2016). Propagation of internal tides on the northwest Australian shelf studied with time-augmented empirical orthogonal functions. In *The Proceedings of the 20th Australasian Fluid Mechanics Conference*. ISBN: 978-1-74052-377-6, paper 744, 4 pgs. Retrieved from https://people.eng.unimelb.edu.au/imarusic/proceedings/20/744%20Paper.pdf

Book, J. W., Perkins, H., Signell, R. P., & Wimbush, M. (2007). *The Adriatic Circulation Experiment winter 2002/2003 mooring data report: a case study in ADCP data processing*. Naval Research Laboratory Memorandum Report. NRL/MR/7330-07-8999, Naval Research Laboratory, 50 pgs.

Deines, K. L. (1999). Backscatter estimation using broadband acoustic Doppler current profilers. In *Proceedings of the IEEE Sixth Working Conference on Current Measurement* (pp. 249–253). IEEE. https://doi.org/10.1109/CCM.1999.755249

Durgesh, V., Thomson, J., Richmond, M. C., & Polagye, B. L. (2014). Noise correction of turbulent spectra obtained from acoustic Doppler velocimeters. *Flow Measurement and Instrumentation*, *37*, 29–41. https://doi.org/10.1016/j.flowmeasinst.2014.03.001

Emery, W. J., & Thomson, R. E. (2001). *Data analysis methods in physical oceanography* (1st ed., Vol. 180). New York: Elsevier. https://doi.org/10.1016/B978-044450756-3/50006-X

Fraedrich, K., Pawson, S., & Wang, R. (1993). An EOF analysis of the vertical-time delay structure of the quasi-biennial oscillation. *Journal of the Atmospheric Sciences*, *50*(20), 3357–3365. https://doi.org/10.1175/1520-0469(1993)050<3357:AEAOTV>2.0.CO;2

Francois, R. E., & Garrison, G. R. (1982). Sound absorption based on ocean measurements. Part II: Boric acid contribution and equation for total absorption. *The Journal of the Acoustical Society of America*, *72*(6), 1879–1890. https://doi.org/10.1121/1.388673

Gostiaux, L., & van Haren, H. (2010). Extracting meaningful information from uncalibrated backscattered echo intensity data. *Journal of Atmospheric and Oceanic Technology*, *27*(5), 943–949. https://doi.org/10.1175/2009JTECHO704.1

Greer, A. T., Shiller, A. M., Hofmann, E. E., Wiggert, J. D., Warner, S. J., Parra, S. M., et al. (2018). Functioning of coastal river-dominated ecosystems and implications for oil spill response: From observations to mechanisms and models. *Oceanography*, *31*(3), 90–103. https://doi.org/10.5670/oceanog.2018.302

Harris, D. C. (2010). *Quantitative Chemical Analysis* (8th ed.). New York, NY: Macmillan.

Heywood, K. J. (1996). Diel vertical migration of zooplankton in the Northeast Atlantic. *Journal of Plankton Research*, *18*(2), 163–184. https://doi.org/10.1093/plankt/18.2.163

Jiang, S., Dickey, T. D., Steinberg, D. K., & Madin, L. P. (2007). Temporal variability of zooplankton biomass from ADCP backscatter time series data at the Bermuda Testbed Mooring site. *Deep Sea Research Part I: Oceanographic Research Papers*, *54*(4), 608–636. https://doi.org/10.1016/j.dsr.2006.12.011

La, H. S., Ha, H. K., Kang, C. Y., Wåhlin, A. K., & Shin, H. C. (2015). Acoustic backscatter observations with implications for seasonal and vertical migrations of zooplankton and nekton in the Amundsen

shelf (Antarctica). *Estuarine, Coastal and Shelf Science*, *152*, 124–133. https://doi.org/10.1016/j.ecss.2014.11.020

Lorke, A., McGinnis, D. F., Spaak, P., & Wüest, A. (2004). Acoustic observations of zooplankton in lakes using a Doppler current profiler. *Freshwater Biology*, *49*(10), 1280–1292. https://doi.org/10.1111/j.1365-2427.2004.01267.x

Parra, S. M., Greer, A. T., Book, J. W., Deary, A. L., Soto, I. M., Culpepper, C., Hernandez, F.J., & Miles, T. N. (2019). Acoustic detection of zooplankton diel vertical migration behaviors on the northern Gulf of Mexico shelf. *Limnology and Oceanography*, *64*(5), 2092–2113. https://doi.org/10.1002/lno.11171

Perkins, H. T., de Strobel, F., & Gualdesi, L. (2000). The Barny sentinel trawl-resistant ADCP bottom mount: Design, testing, and application. *IEEE Journal of Oceanic Engineering*, *25*(4), 430–436. https://doi.org/10.1109/48.895350

Richard, J.-B., Thomson, J., Polagye, B. L., & Bard, J. (2013). Method for identification of Doppler noise levels in turbulent flow measurements dedicated to tidal energy. *International Journal of Marine Energy*, *3–4*, 52–64. https://doi.org/10.1016/j.ijome.2013.11.005

Teledyne RDI. (2010). *ADCP coordinate transformation: Formulas and calculations*.

Teledyne RDI. (2011). *Acoustic Doppler current profiler: Principles of operation. A practical primer*.

Table 1. Instrument and measurement details at the five longer-term moorings of the acoustic Doppler current profilers (ADCPs) and wave and tide gauges (WTG) (Figure 1). All times are in Universal Time Coordinated (UTC).

	C1	*C2*	*C3*	*C4*	*C5*
Latitude, 29° N	16.85’	16.95’	16.90’	20.10’	21.74’
Longitude, 88° W	49.35’	41.16’	33.45’	47.71’	40.95’
Deployment: November 2015	Day 3rd: 00:51	Day 2nd: 23:07	Day 3rd: 15:59	Day 3rd: 02:21	Day 3rd: 14:32
Recovery: April 13th, 2016	15:58	18:01	19:22	14:19	12:33
Depth (m)	59	65	68	46	56
			ADCPs		
Frequency (kHz)	300	300	300	600	300
Bin size (m)	1	1	1	1.5	1
Top bin depth (m)	4	4	4	5	4
Ping interval (s)	4	4	4	0.5	4
Pings/ensemble	3	3	3	2	3
Ensemble interval (s)	12	12	12	1	12
Burst interval	-	-	-	1 h	-
Burst duration	-	-	-	10 min	-
			WTG		
Temperature, conductivity, pressure interval (min)	failed	10	20	10	10

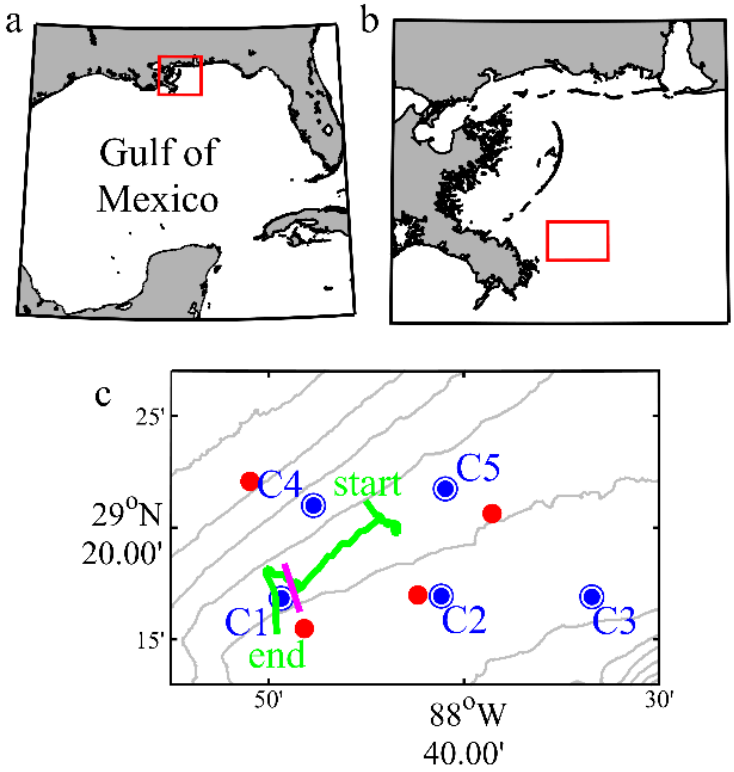

Figure 1: Map of the study site within the Gulf of Mexico. The red rectangles in (a) and (b) show the location of the Mississippi Bight within the Gulf of Mexico and the study site east of the Mississippi River Bird's Foot Delta, respectively. (c) The site was studied using five bottom moorings (blue circles) and glider data along the green track, with day and night measurements of zooplankton using In Situ Ichthyoplankton Imaging System (ISIIS) tows (magenta line) and net tows (red circles). The gray lines represent bathymetric contours every 10 m starting at 20 m at the northwest corner. The package M_Map was used to create the maps (www.eoas.ubc.ca/~rich/map.html). From Parra et al. (2019), Figure 1.

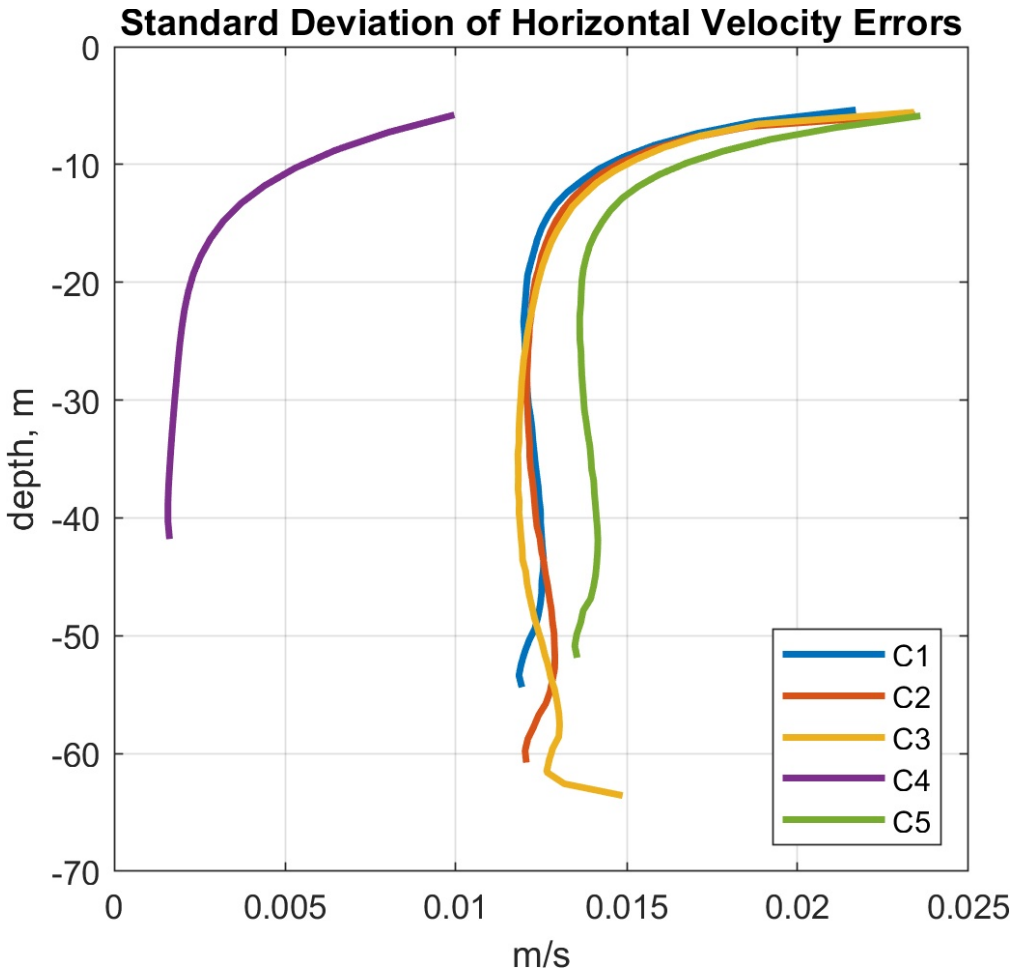

Figure 2: Standard deviation profiles of the horizontal error velocities using equation (5) for all the moorings.

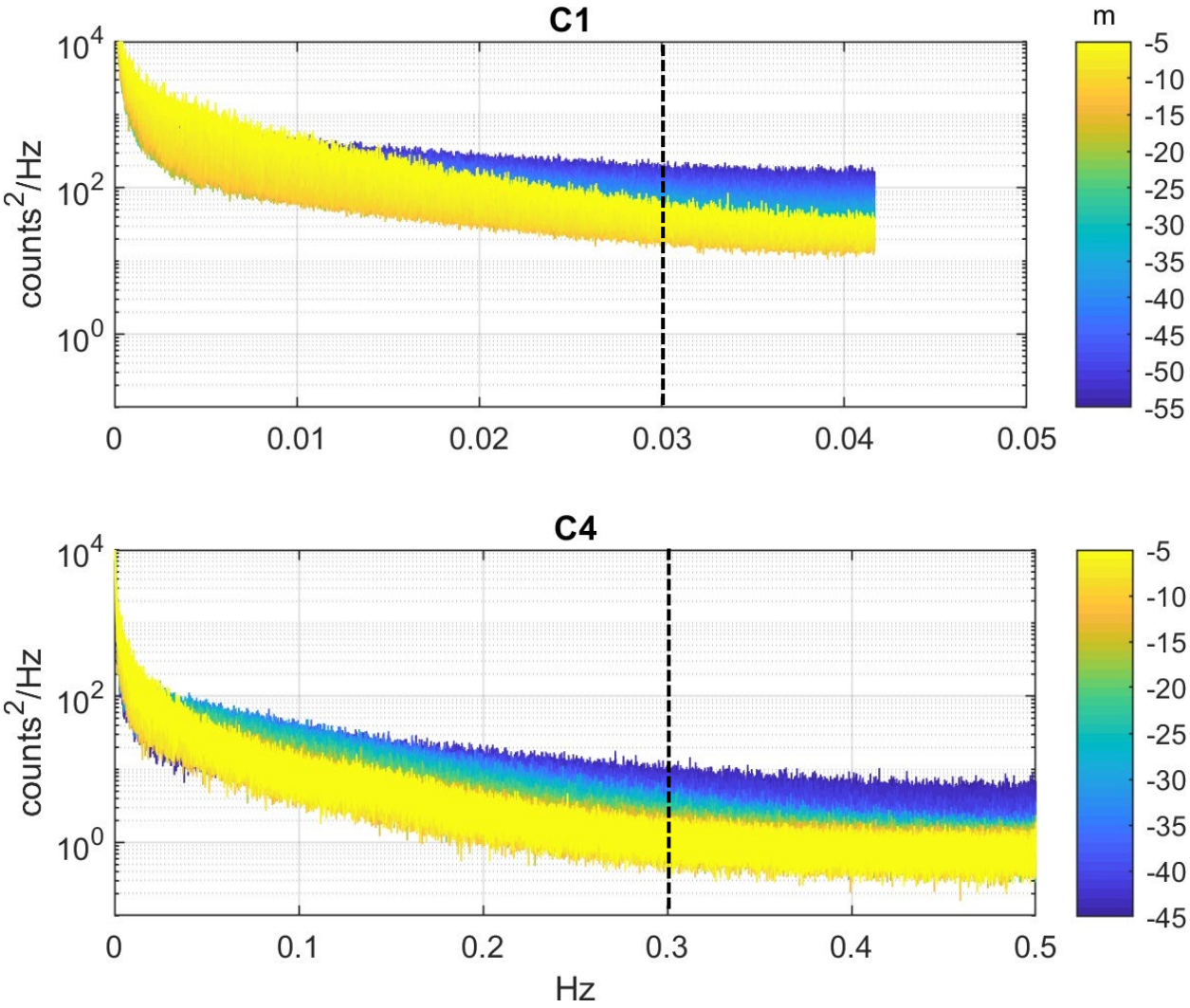

Figure 3: Spectrum of the echo intensity at C1 and C4 for each depth level. The colorbar denotes the depth of each spectrum. The dashed black lines represent the cutoff frequency. Note the different x-axis range between the two plots.

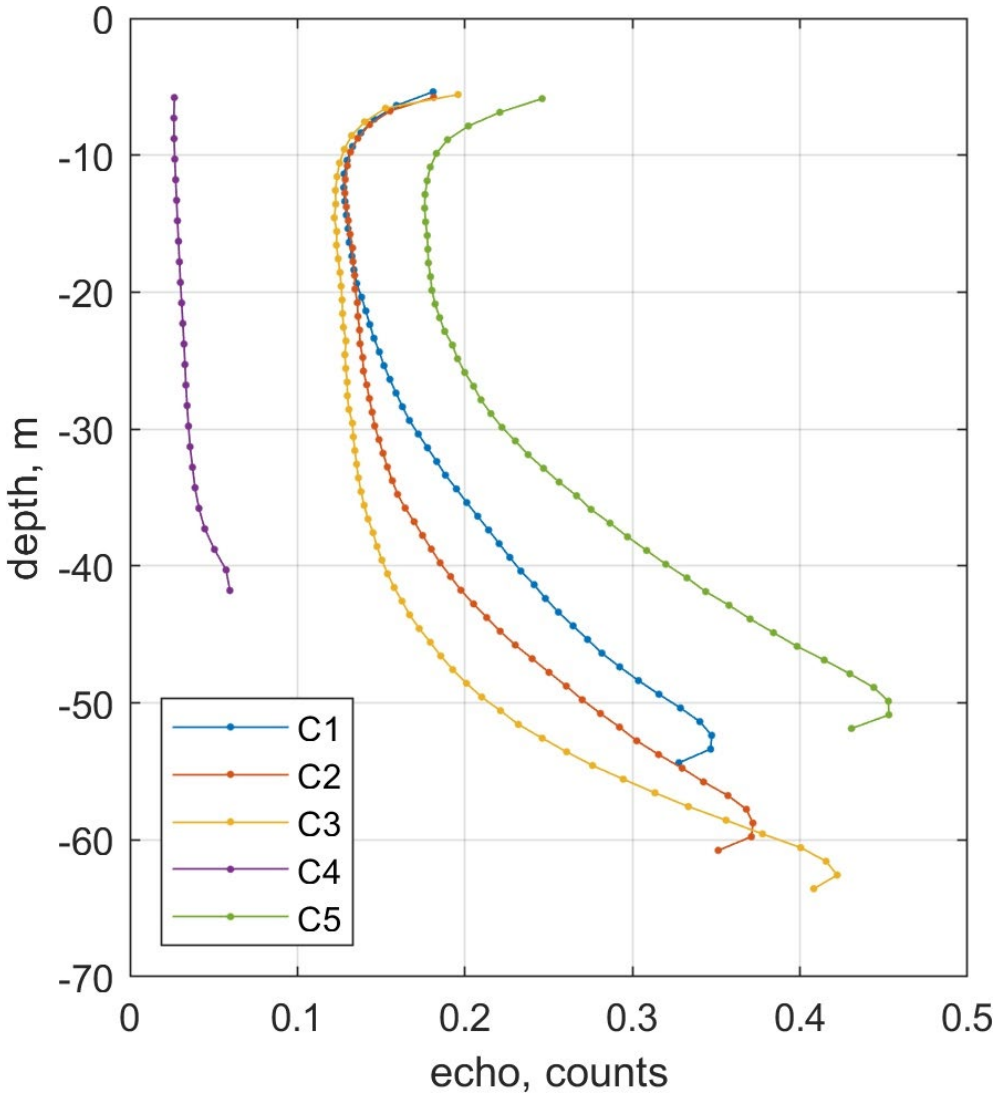

Figure 4: Profiles of the echo error at each mooring calculated using equation (7) using the spectral white noise floor.

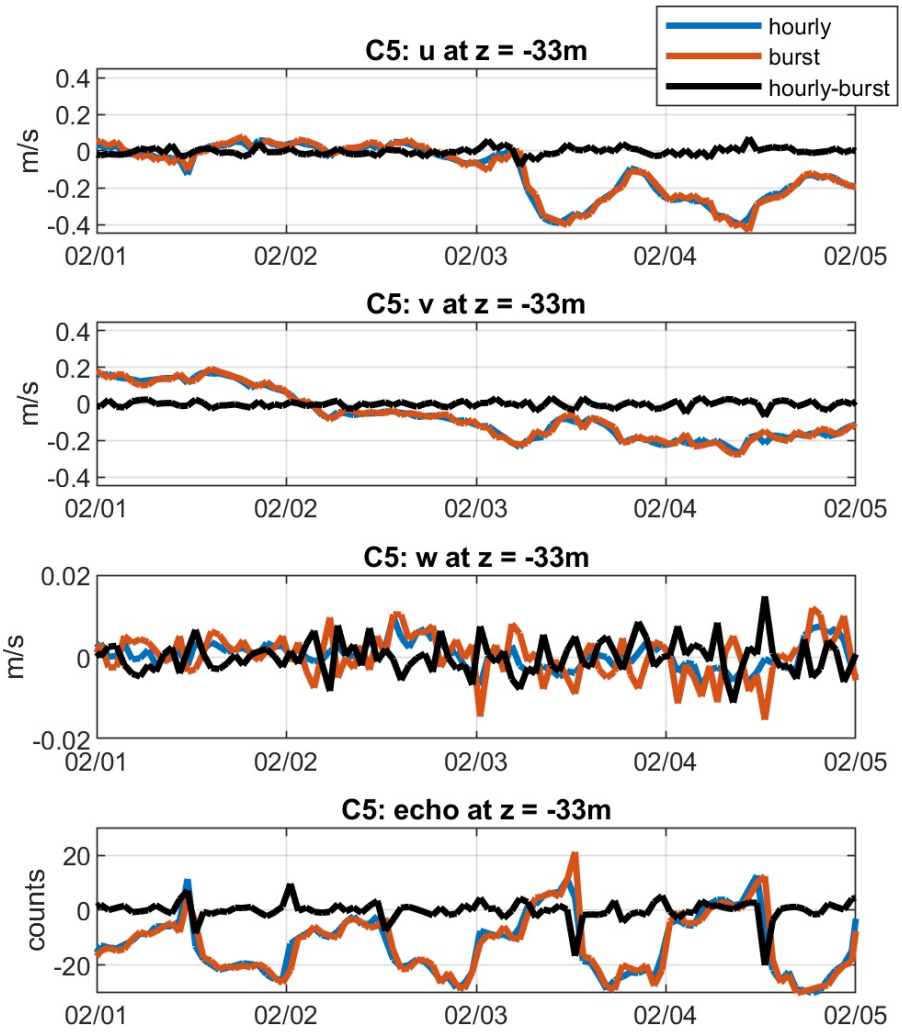

Figure 5: Time series of east (u), north (v) and vertical velocities (w), and demeaned echo intensity (echo) at a depth of 33 m (mid water column) at C5. Comparison between two sampling schemes: hourly averages of continuous data (blue), and hourly burst sampling represented by the average of the first 10 minutes of each hour (orange). The difference between these two is the black line, and is an indicator of the burst sampling error. Time is in Universal Time Coordinated (UTC).

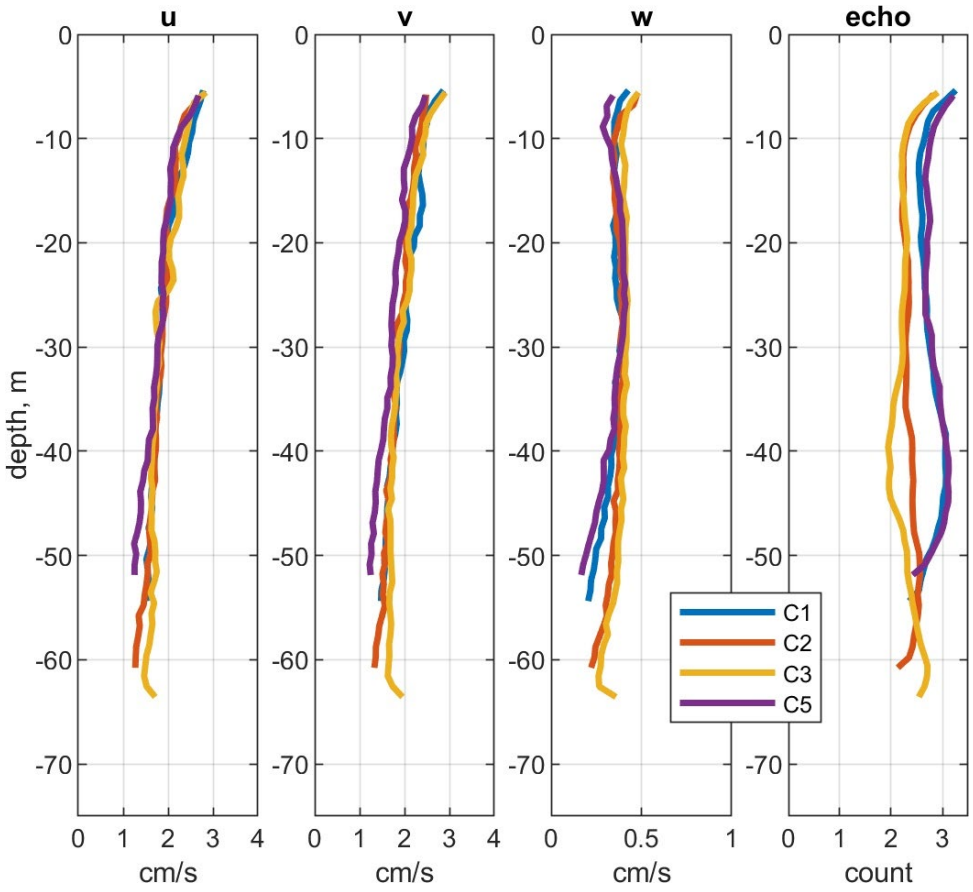

Figure 6: Error profiles estimated for the C4 burst measurement scheme using equation (8) and data from the moorings that measured continuously for variables east (u), north (v) and vertical velocities (w), and echo intensity (echo).

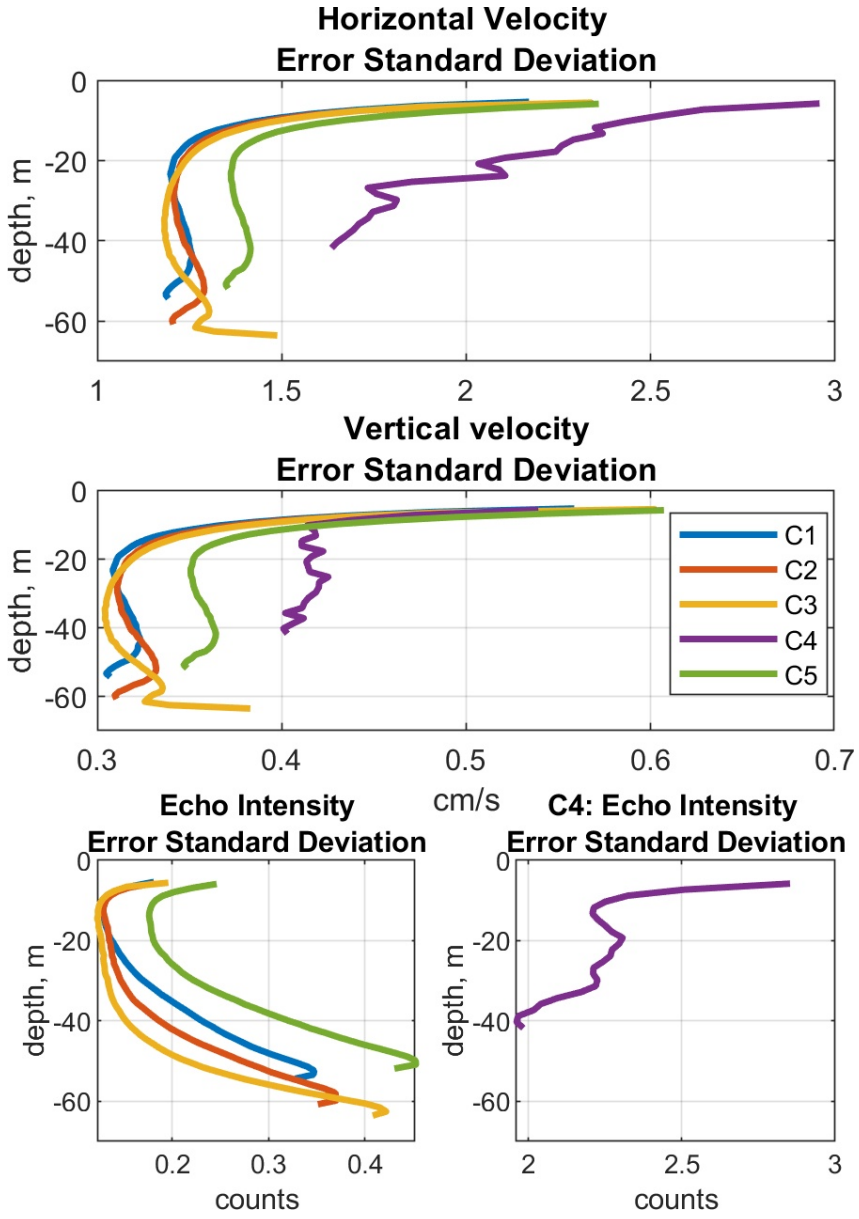

Figure 7: Error profiles for the horizontal and vertical velocities, and echo intensity, which includes the burst sampling error at C4. Note the different scale of the echo error at C4 relative to the other moorings.

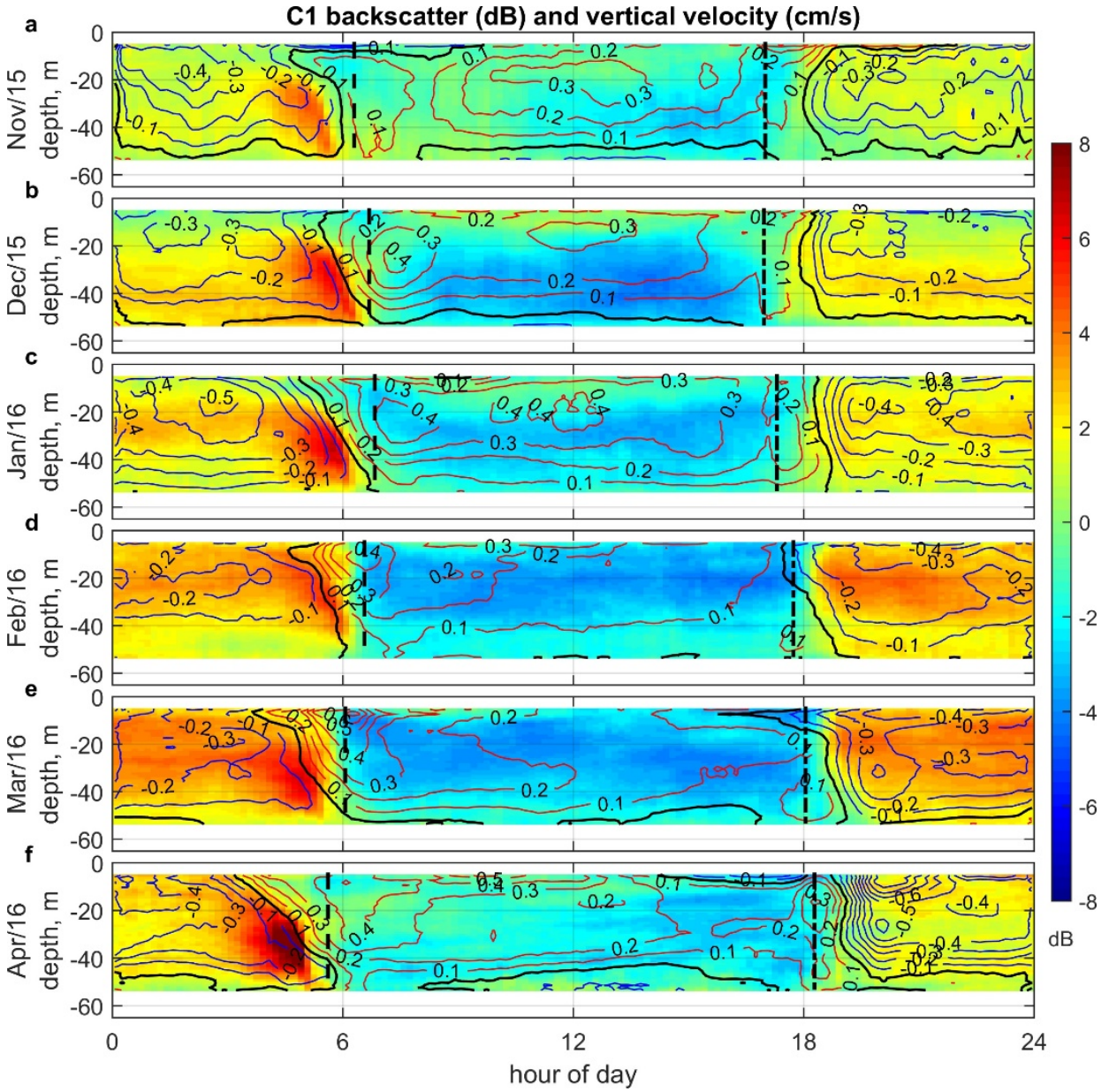

Figure 8: Monthly mean of the daily relative backscatter anomaly (filled contours) overlain by the high-pass filtered vertical velocities (contour lines) at C1 plotted as a function of hour of day in Universal Time Coordinated minus 6 hours (UTC-6) and depth. The red contour lines represent positive vertical velocities, black is zero, and blue are negative vertical velocities. Each row represents a different month from (a) November 2015 through (f) April 2016 with the average sunrise (dashed) and sunset (dot dash) times for each. From Parra et al. (2019), Figure 4.

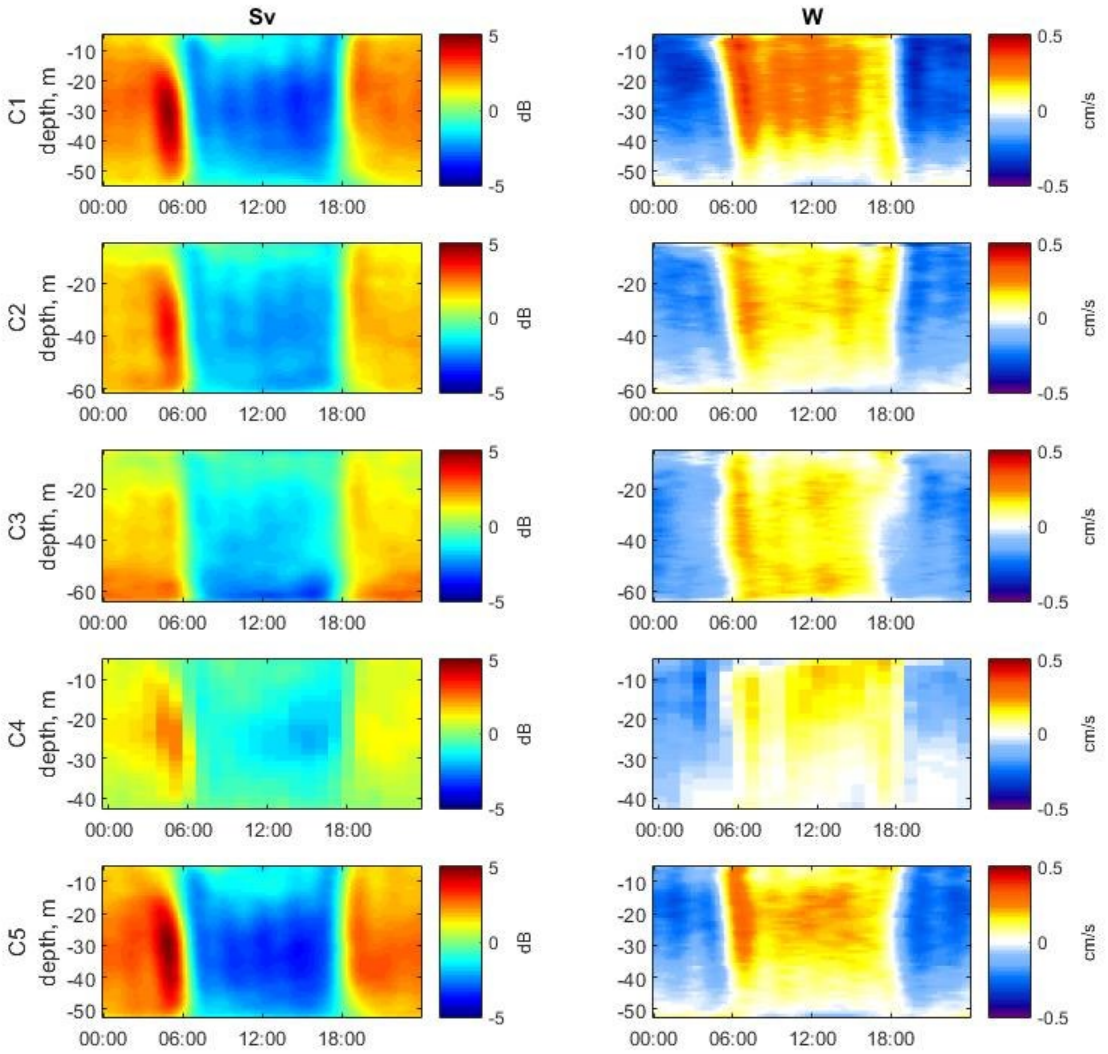

Figure 9: Overall daily averages (over the deployment duration) of relative backscatter anomaly, S_v, and vertical velocity, W, at each mooring. Horizontal axis is local hour of the day (UTC – 6 hours).

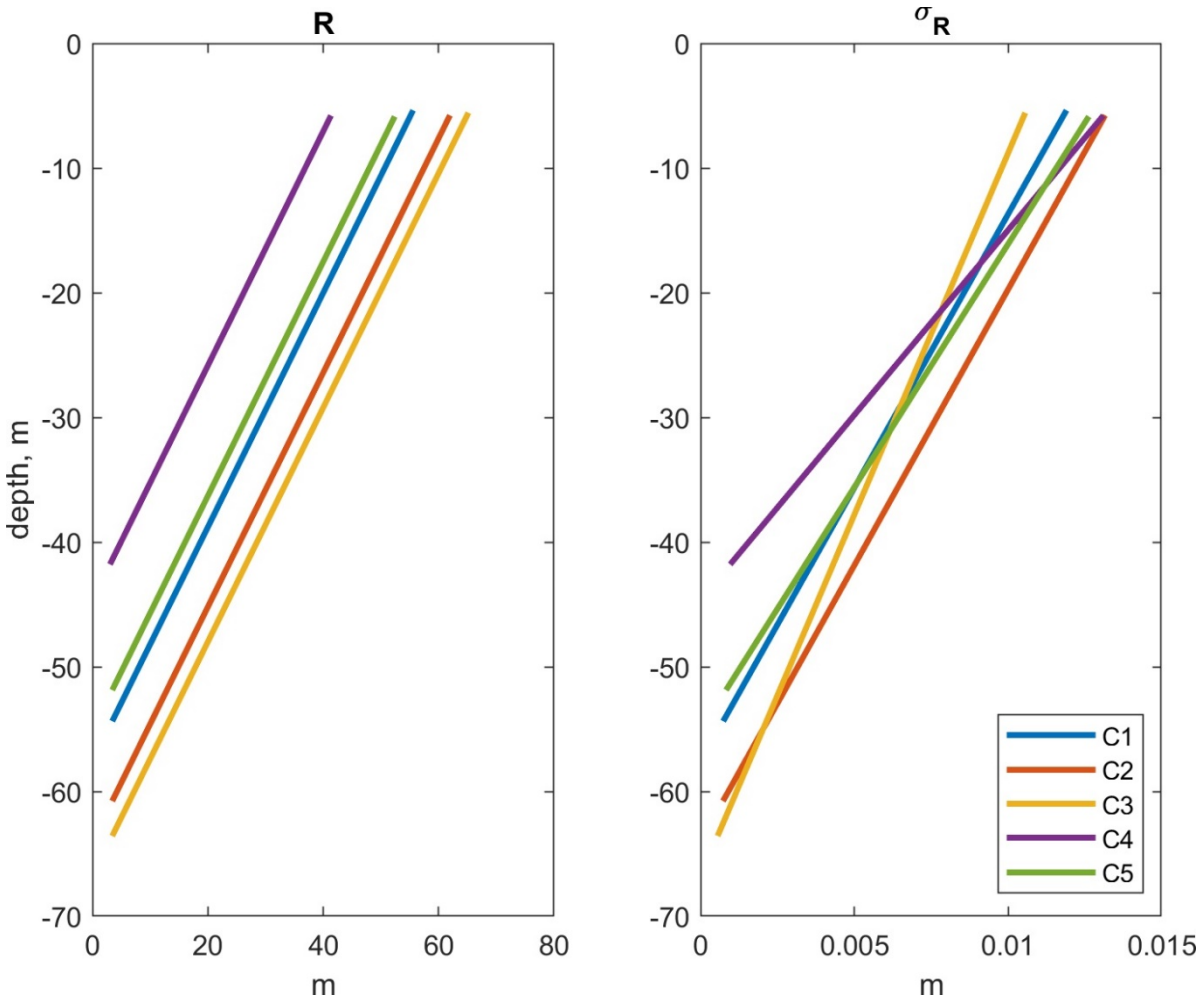

Figure 10: Profiles of *R* (left) and error associated with *R* (right) for each mooring (same color coding as previous figures).

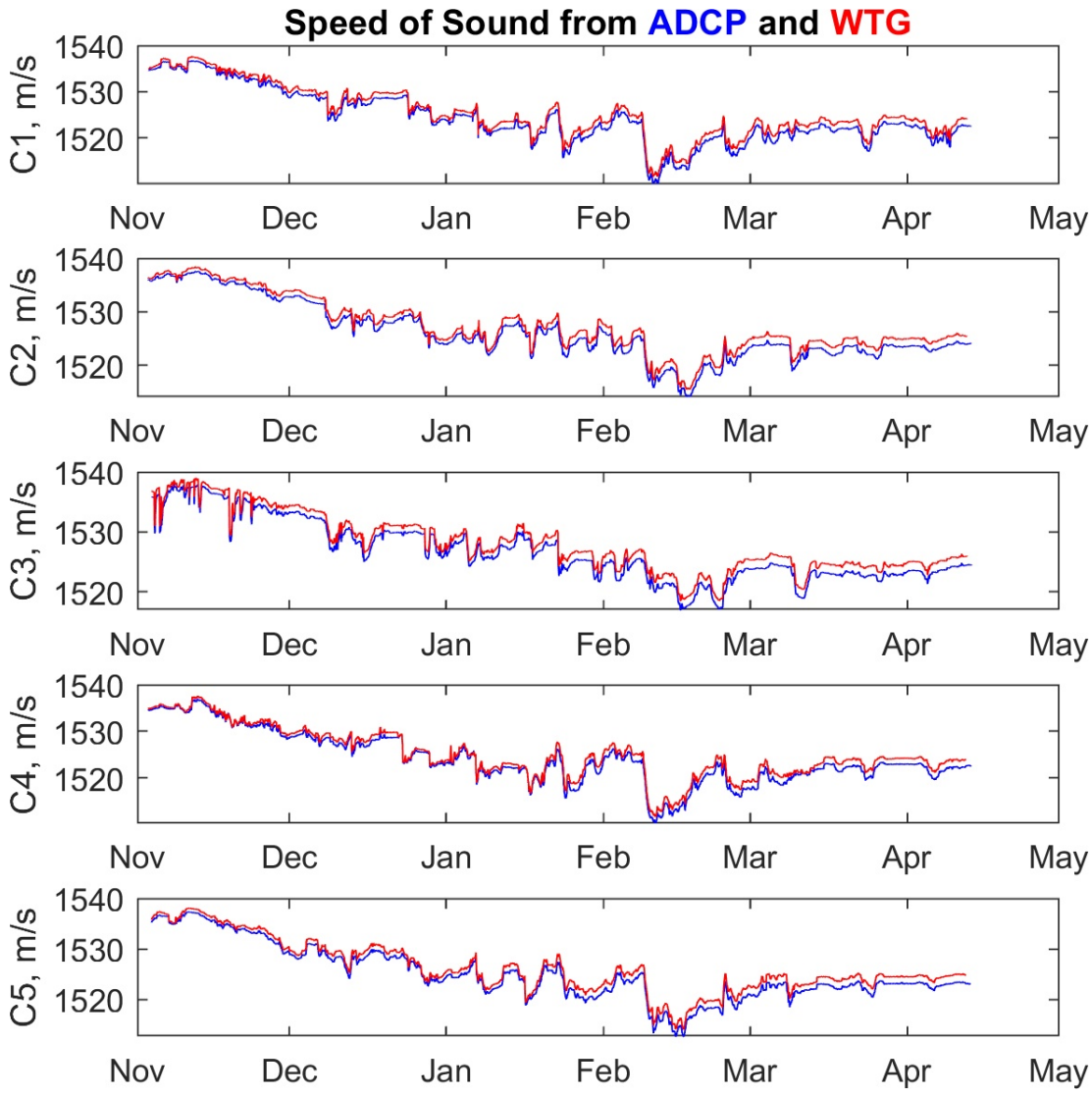

Figure 11: Speed of sound as estimated by the ADCP (blue) and calculated using a wave-tide gauge (red) at all the moorings except C1. The WTG estimate at C1 used salinity time series from the WTG at C2.

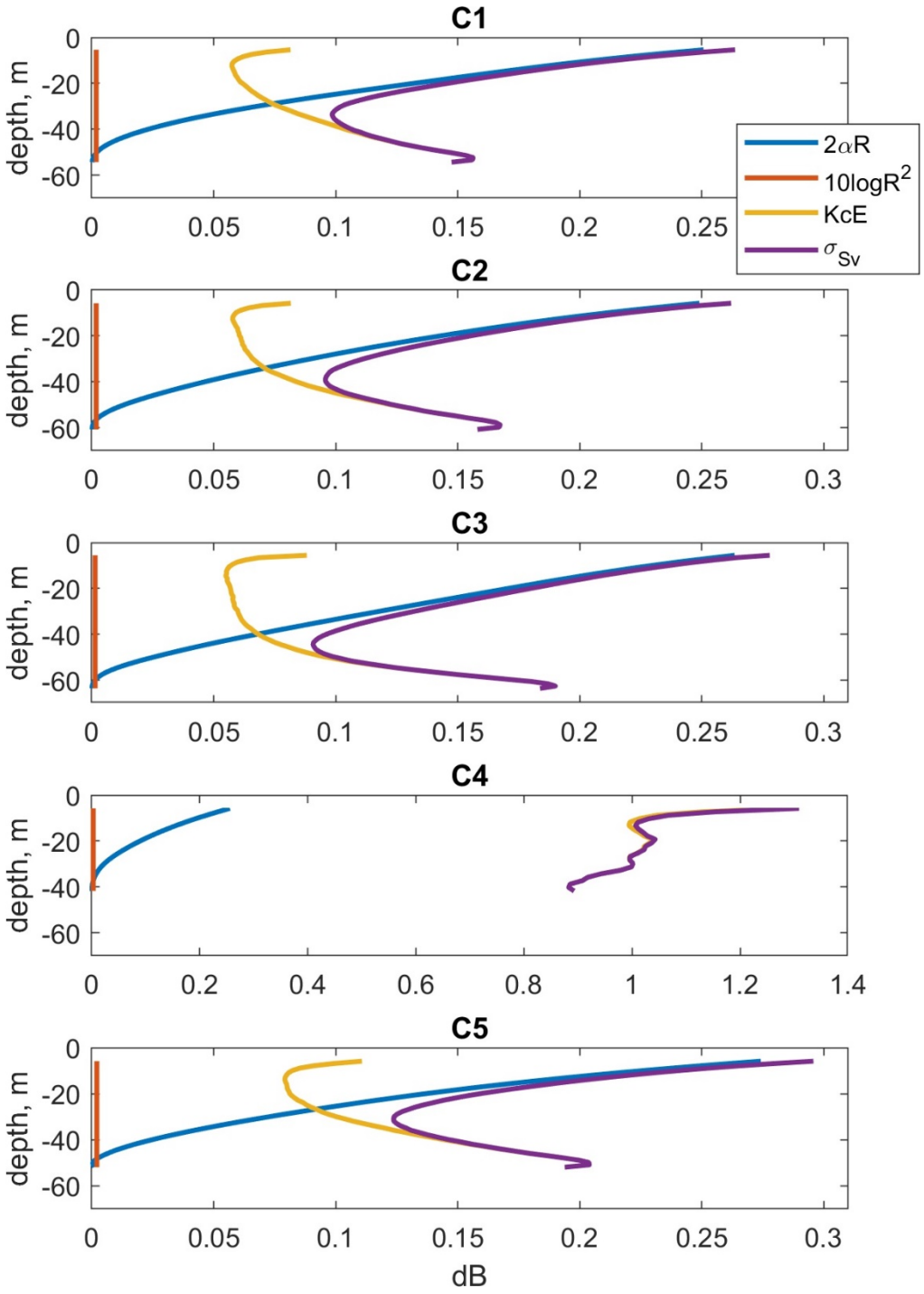

Figure 12: Error profiles of the backscatter equation terms (right hand side of equation 12) and the profile of the sum of the backscatter errors (purple) at all the moorings. Note the different x-axis scale at C4.

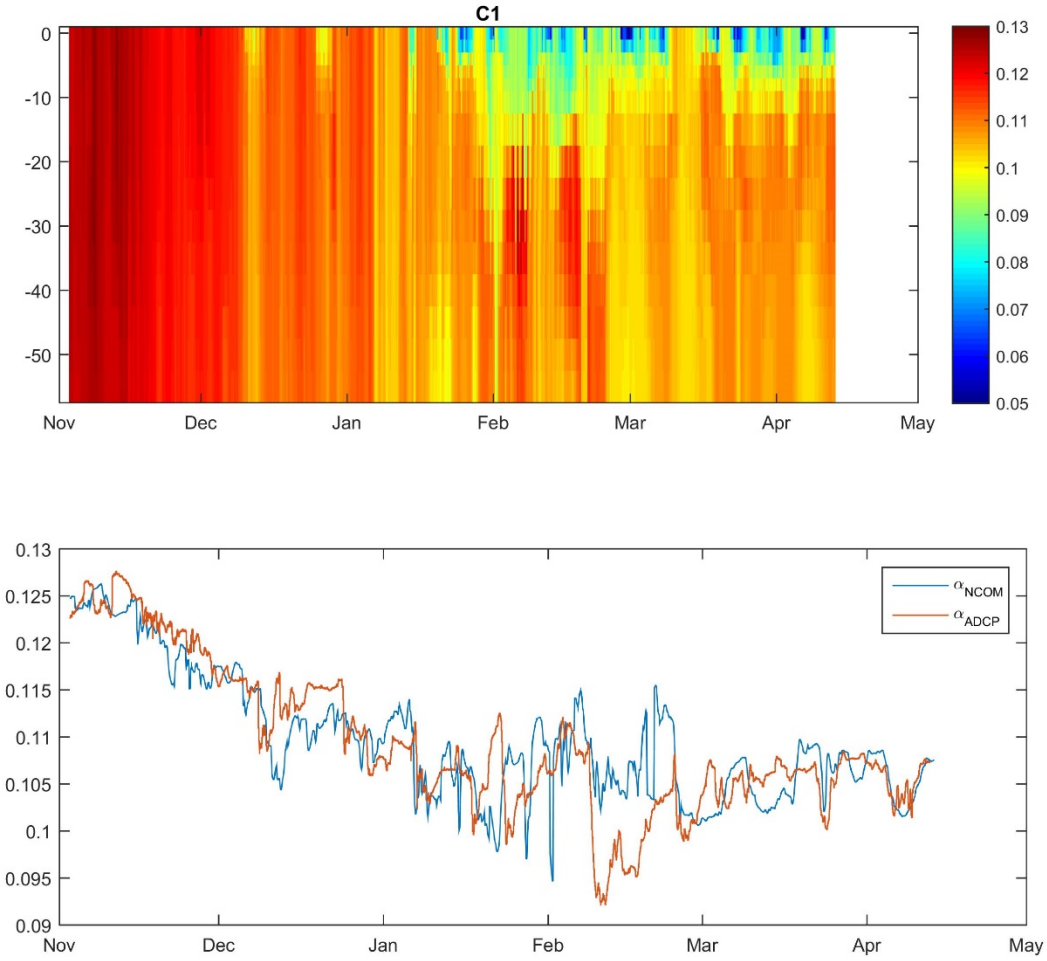

Figure 13: (above) Profiles of sound absorption of seawater, α (dB/m), at C1 as estimated from a numerical model of this region (for a description of the Navy Coastal Ocean Model that was used see Greer et al., 2018). Vertical axis is depth in m. (below) Time series of sound absorption of seawater at the bottom at C1 from the model (blue) and as calculated from the bottom ADCP and WTG (orange). Vertical axis is dB/m.

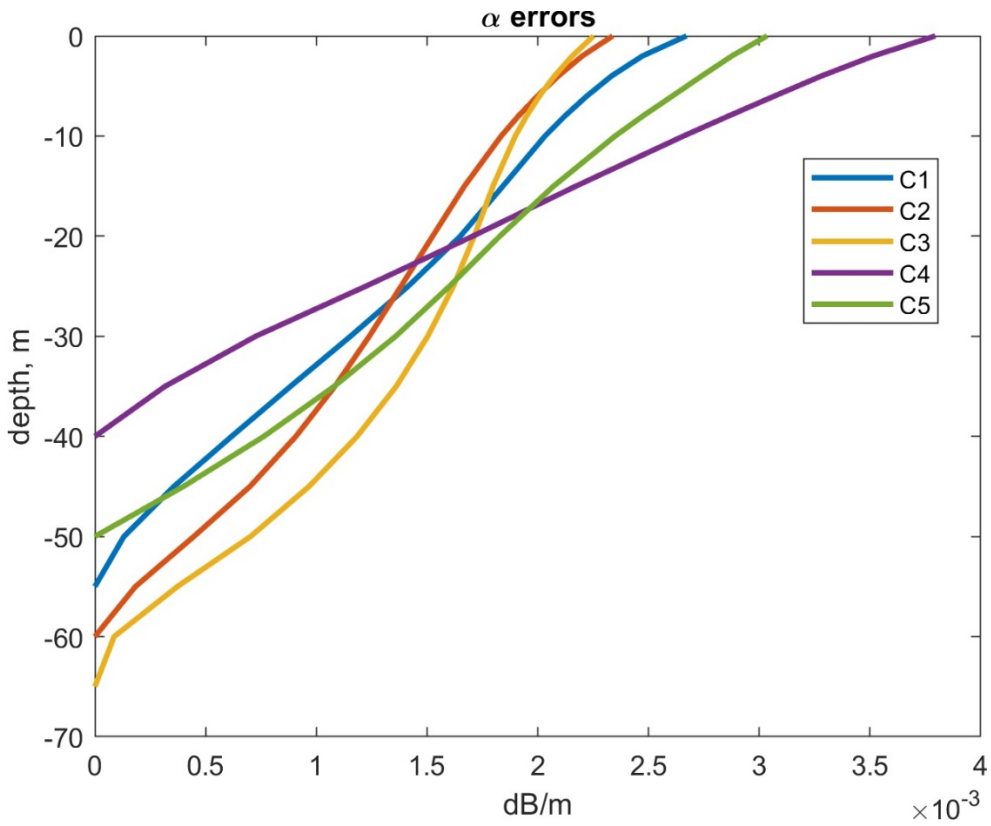

Figure 14: Error profiles associated with the sound absorption of seawater, α, at all the moorings using equation (18).

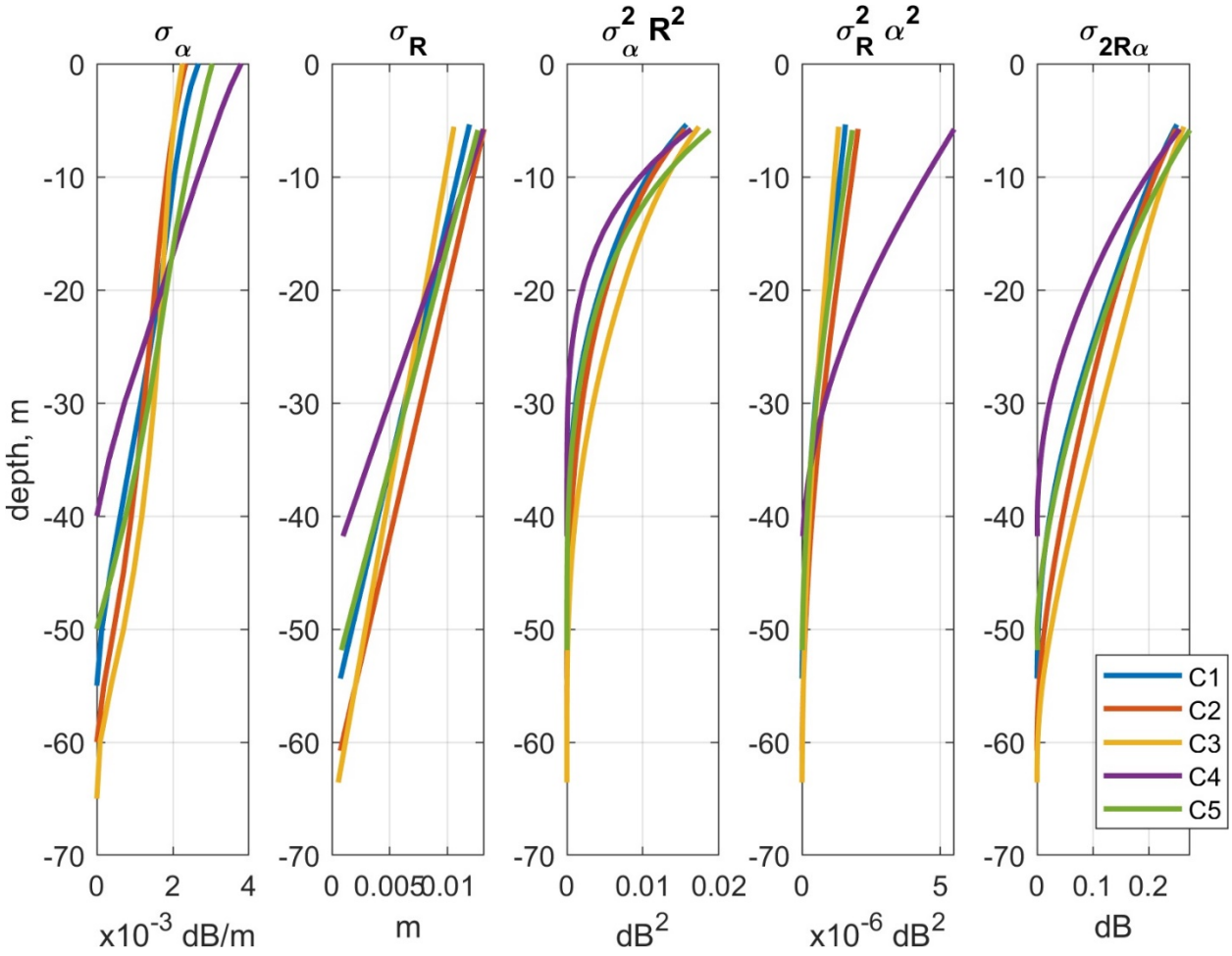

Figure 15: Error profiles at each mooring for the second term of the right hand side of equation (12), separated by the different variables used in equation (19).

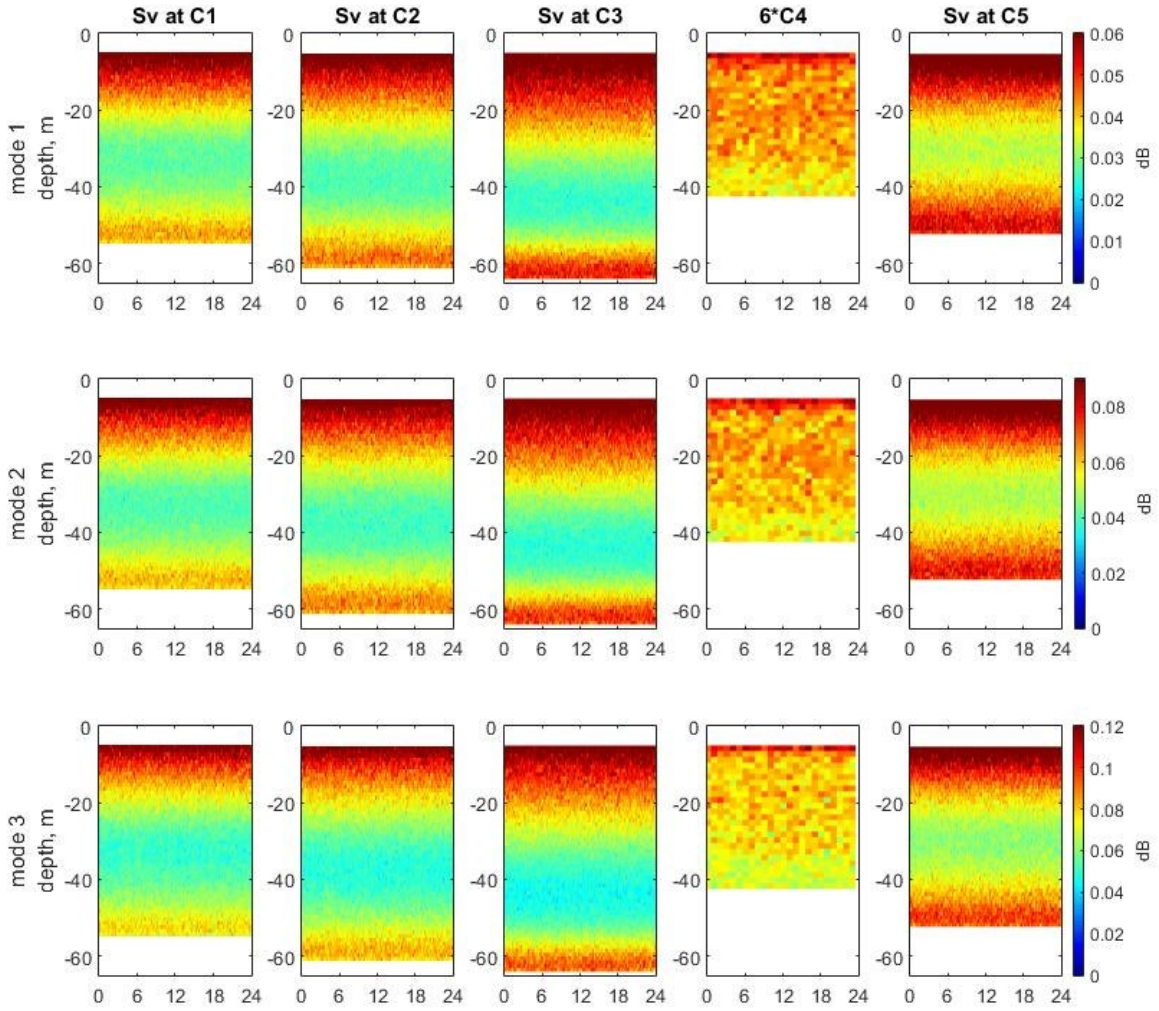

Figure 16: EOF errors of the relative backscatter anomaly for each mode and each mooring. Each mode (rows) has a different colorbar scale. The color range at C4 was divided by 6 to conform with the colorbars for each mode. This was calculated using equation (21). Horizontal axis is local hour of the day (UTC – 6 hours).

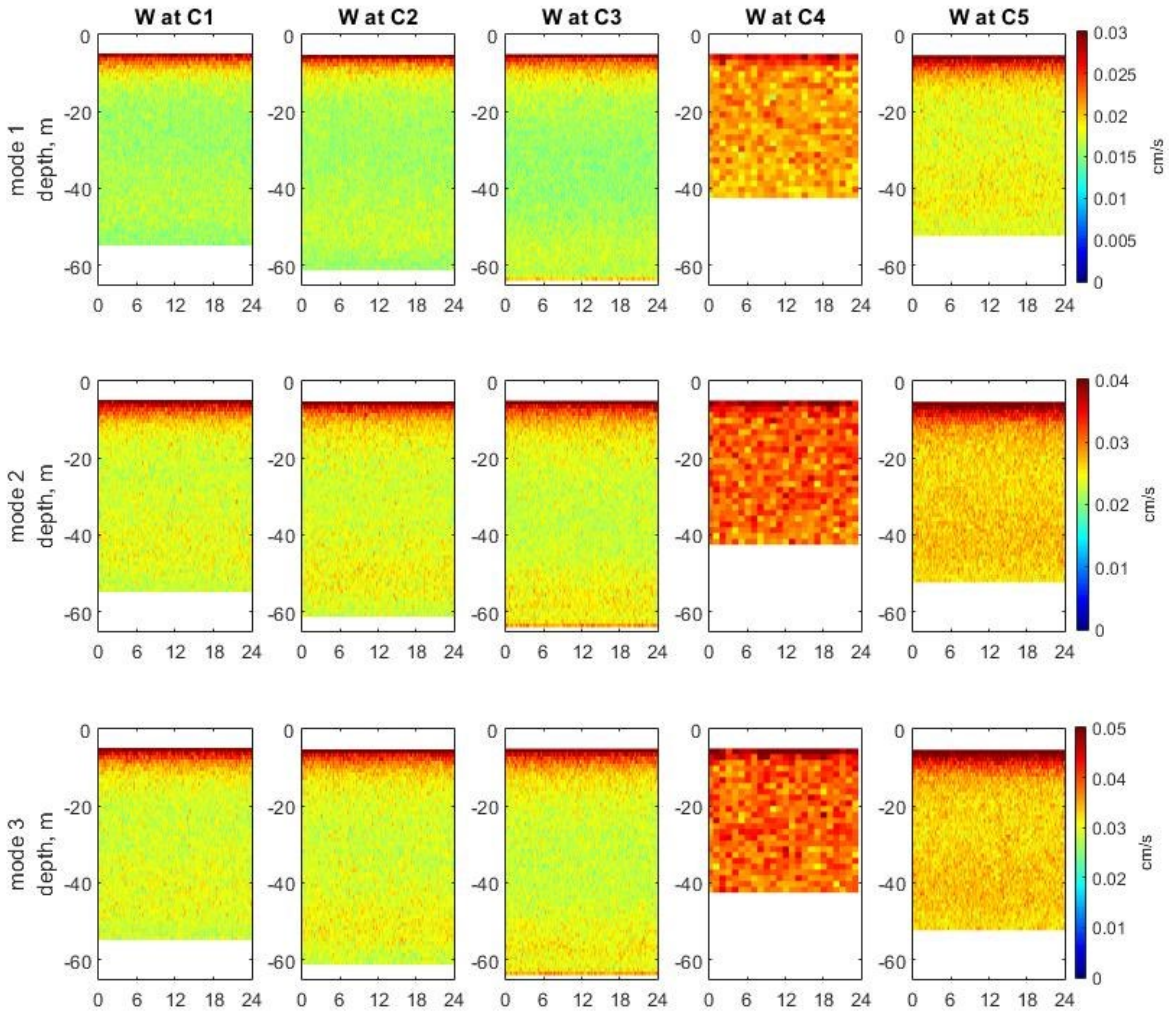

Figure 17: EOF errors of the vertical velocities for each mode and each mooring. Each mode (rows) has a different colorbar scale. This was calculated using equation (21). Horizontal axis is local hour of the day (UTC – 6 hours).

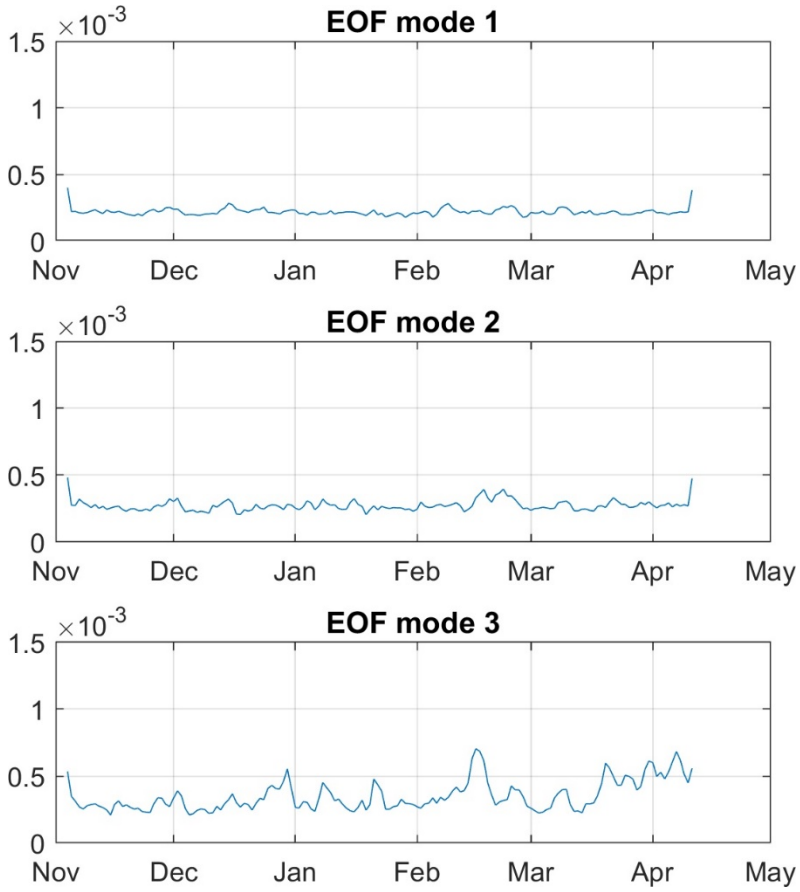

Figure 18: EOF errors of the temporal amplitudes for each mode (unitless). This was calculated using equation (21).